ISSN 0020-4412, Instruments and Experimental Techniques, 2015, Vol. 58, No. 1, pp. 1–14. © Pleiades Publishing, Ltd., 2015.
Original Russian Text © A.B. Tolstogouzov, S.F. Belykh, V.S. Gurov, A.A. Lozovan, A.I. Taganov, O.M.N.D. Teodoro, A.A. Trubitsyn, S.P. Chenakin, 2015, published in Pribory i Tekhnika Eksperimenta, 2015, No. 1, pp. 5–20.

Ion-Beam Sources Based on Room-Temperature Ionic Liquids for Aerospace Applications, Nanotechnology, and Microprobe Analysis (Review)

A. B. Tolstogouzov[a, b], S. F. Belykh[c], V. S. Gurov[b], A. A. Lozovan[c], A. I. Taganov[b], O. M. N. D. Teodoro[a], A. A. Trubitsyn[b], and S. P. Chenakin[d]

[a] *Center for Physics and Technological Research, Dept. de Física da Faculdade de Ciênciase Technologia Universidade Nova de Lisboa, Campus de Caparica, 2829-516 Caparica, Portugal*
e-mail: a.tolstoguzov@fct.unl.pt
[b] *Ryazan State Radio Engineering University, ul. Gagarina 59/1, Ryazan, 390005 Russia*
[c] *Tsiolkovskii Russian State Technological University, ul. Polbina 4, Moscow, 109380 Russia*
[d] *Kurdyumov Institute for Metal Physics, National Academy of Sciences of Ukraine, bul. Akademika Vernadskogo 36, Kyiv, 03680 Ukraine*

Received March 26, 2014

Abstract—An analytical review of the stages of development and the modern state of development of ion-beam sources, which are based on room-temperature ionic liquids for aerospace and ion-beam technologies, is presented. The properties of ionic liquids—new ion-conducting materials ("liquid plasma or plasma in a bottle")—are discussed. The design, operating conditions, and technology of manufacturing pointlike, capillary, matrix, and linear ion sources with ionic liquids are described in detail. The main fields of their application, including electrostatic rocket engines (microthrusters) for CubeSat-format satellites and systems with sharply focused ion beams for technological processing of materials and structures in the nanometer region and for microprobe investigations are analyzed.

DOI: 10.1134/S002044121501011X

1. INTRODUCTION

This review is devoted to ion-beam sources (ion guns), in which room-temperature ionic liquids are used as the working substances. It should be noted that here we do not consider ion-beam sources (ISs) that are used in the analysis of liquid analyts in modern mass spectrometers, e.g., in instruments with ion extraction from solutions in electric fields. Our attention will be drawn to the principles of operation and specific design features of ISs for small electrostatic propulsion engines (ionic microthrusters), for technological processing of materials and structures in the micro- and nanometer ranges, and for analytical microprobe systems, primarily, for secondary-ion mass spectrometry (SIMS).

Any melts of salts, e.g., sodium chloride at $T >$ 800°C, can be classified as ionic liquids in the wide meaning of this term. Melts of organic salts with melting temperatures $T < 100$°C attract the greatest interest among numerous substances in the class of ionic liquids [1–3]. Hereinafter, the term "ionic liquids" will mean exactly room-temperature ionic liquids (RTILs).

As a rule, the RTIL composition includes a complex bulk organic cation, while an anion may be either inorganic or organic. Varying cations and anions allows changes in the RTIL characteristics, such as the melting temperature, viscosity, electrical conductivity, wettability, etc. As a result of their ionic nature, RTILs are characterized by an extremely low pressure of saturated vapors, thus allowing their use even under ultrahigh-vacuum conditions. RTILs remain to be liquid in a wide temperature range and have high thermal stability. They are not inflamed, their toxicity is low, and many of them are inert with respect to air and water.

At present, more than 5000 various RTILs are known, and new compounds are being successfully synthesized [4]. The first report on a salt that is liquid at room temperature (ethyl ammonium nitrate $[EtNH_3]^+[NO_3]^-$) was published in 1914 by Russian chemist P.I. Valden [5]. In recent years, RTILs became very popular in the field of organic synthesis and metal-complex catalysis; they are considered to be ideal solvents for "green" chemistry and are used in electrochemical sensors, fuel elements, and accumulators, during electrodeposition, cleaning, and electropolishing of metals. Detailed descriptions of various fields of application of RTILs can be found in [6–9]. As far as we know, in Russia, ion liquids are investi-

gated mainly by chemists (e.g., see the page of the editor-in-chief of the Journal of Analytical Chemistry [10]), and the issues of the development and application of ISs with ionic liquids (ILIS) have not still been discussed in the domestic scientific literature.

From the standpoint of the design and operating principles, liquid-metal (electrohydrodynamic) ion sources (LMISs) are the closest to ILISs [11–13]. In LMILs, metals with low melting temperatures (gallium, indium, and cesium) and eutectic alloys that are based on gold, bismuth, manganese, and other metals are used as the working substances [14].

A small part of the liquid-metal (alloy) surface, which wets and covers a metal needle or the outlet hole of a capillary with a thin layer, serves as the ion emitter in an LMIS. The extracting electrode creates an electric field with a strength of 10^8 V/cm near the emitter, and ions (atomic and cluster) with different charge multiplicities together with neutral excited atoms and neutral and positively charged liquid-metal drops are emitted from the vertex of the Taylor–Hilbert cone (which is also called the Taylor cone), which is the liquid-metal surface at each point of which the actions of the electric field and the metal-surface tension are balanced. The field evaporation is considered to be the main process that is responsible for the emission phenomena in LMISs. The principles and conditions of operation of LMISs were considered in detail in [11, 12].

Owing to the high brightness (~10^6 A cm^{-2} sr^{-1}) and the small energy spread (5–10 eV), LMISs allow one to obtain sharply focused ion beams with a diameter of <10 nm and a current density of up to 30 A/cm^2 (for an accelerating voltage of 20–30 kV). Gallium-based LMISs (focus ion beam, FIB) [13, 15] are widely used in ion lithography, during precise mechanical microprocessing (milling), manufacturing and retouching of photomasks and X-ray masks, reactive ion etching, and in microscopy and microanalysis using the SIMS method. Various LMISs for technological and analytical applications were developed in the USSR (e.g., [16–18]) with participation of the authors of the present review.

Studies on the development of indium- and cesium-based LMISs for aerospace application have been performed since the end of the 1960s. The first tests of an indium LMIS that was developed within the framework of the joint Soviet–Austrian project LOGION were carried out in 1991 at the *MIR* space station [19]. Subsequently, LMISs (mainly with indium) were used at different space stations as sources of probing beams in ion microanalyzers (e.g., the MIGMAS project) and for compensating for electrostatic charging of the spacecraft surfaces appearing under the action of a "solar wind."

To date, microthrusters with metallic cesium as the working substance have been developed and are ready to be tested on a circumterrestrial orbit [20]. In these apparatuses, Cs^+ ions are accelerated under the action of an electrostatic field to high velocities and produce a controlled propulsive force (thrust) within a range from micro- to millinewtons. The main purpose of microthrusters is the precise correction of the orbits of small-size spacecrafts with weights of 1–10 kg. In the domestic literature, microthrusters belong to the group of electric rocket engines [21], whereas in the Anglo–American literature, they are classified as field electric emission propulsion (FEEP) systems [22].

Similar to liquid metals, RTILs can be used in the generation of ion beams that are required in all the aforementioned fields. Let us briefly enumerate the main advantages of RTIL-based sources in comparison to LMISs. ILISs can generate beams of both positively and negatively charged ions with different masses, including those with masses that exceed 5000 amu. LMISs are fundamentally unable to emit negative ions, and the mass of even very heavy metal cluster ions, e.g., Bi_7^+, does not exceed 1500 amu. Heavy cluster ions of positive and negative polarities are important during the SIMS analysis of complex organic compounds, because they provide preservation of the molecular structures of analyzed substances [23].

The operating voltage for ILISs is lower than that for LMISs because of a lower surface tension for ionic liquids; in addition, it becomes unnecessary to even slightly heat ionic liquids, while in the case of liquid metals and alloys, it is impossible to manage without heating. These advantages are especially important for micro-, nano-, and picosatellites with limited onboard resources.

During local reactive (chemical) ion etching (chemical or gas-assisted FIB etching) [24, 25], fluorine-, chlorine-, and oxygen-containing active gases are let into the working chamber, and the sample surface is irradiated with a focused beam of gallium ions. Under such conditions, a considerable increase in the sputtering coefficient (etching efficiency) is observed for many materials with a simultaneous decrease in the effect of deposition of the sputtered substances, because when the latter enter into chemical reactions with the working gases, the latter form volatile radical compounds, which are efficiently evacuated from the working chamber using vacuum pumps. Contaminating the sample surface with gallium and active gases, which precipitate on its surface, is a disadvantage of the reactive-etching procedure. Moreover, the gallium-ion beam may be defocused during its passage through a gas-filled volume as a result of scattering during collisions of primary ions with gas molecules, thus impairing the local resolution of this method and reducing the etching efficiency. The application of ILISs will allow local chemical etching to be performed without the admission of active gases, because beams of primary ions may contain chlorine, fluorine, and oxygen compounds. The use of negatively charged heavy cluster ions minimizes the surface-charging

Table 1. Some RTILs that are used in ISs (chemical formulas and molecular masses of cations and anions, which enter into the composition of these RTILs)

Ionic liquid	Abbreviated notation	Molecular mass, amu		
		$[R]^+[A]^-$	$[R]^+$	$[A]^-$
1-Ethyl-3methylglyoxaline tetrafluoroborate	[emim][BF_4]	$C_6H_{11}N_2BF_4$ 197.98	$C_6H_{11}N_2$ 111.17	BF_4 86.81
1-Ethyl-3-methylglyoxaline bis(trifluormethyl-sulfonyl)imid	[emim][Tf_2N]	$C_8H_{11}N_3O_4S_2F_6$ 391.31	$C_6H_{11}N_2$ 111.17	$N(SO_2CF_3)_2$ 280.14
1-Butyl-3-methylglyoxaline bis(trifluormethyl-sulfonyl)imid	[bmim][Tf_2N]	$C_{10}H_{15}N_3O_4S_2F_6$ 419.36	$C_8H_{15}N_2$ 139.22	$N(SO_2CF_3)_2$ 280.14
1-Butyl-3-methylglyoxaline hexafluorinephos-phate	[bmim][PF_6]	$C_8H_{15}N_2PF_6$ 284.18	$C_8H_{15}N_2$ 139.22	PF_6 144.96

effect; i.e., it becomes unnecessary to have an additional electron source for neutralizing this charge.

Summarizing the above, it can be asserted that a new promising trend in the ion-beam and aerospace technologies and microprobe analysis has been formed. This trend is based on ion sources with liquid ion-conducting working substances, RTILs.

2. IONIC LIQUIDS FOR ION SOURCES: THE BASIC PROPERTIES

As was mentioned above, RTILs consist of organic cations $[R]^+$ and organic or inorganic anions $[A]^-$. However, RTILs should not be considered as homogeneous liquid mixtures of cations and anions. According to the modern theoretical and experimental conceptions (see, e.g., [26, 27] and references herein), RTILs are complex nanostructured liquids that consist of polar and nonpolar regions with ordered structured: domains, ion vapors, quasi-molecular packages, and associates.

It was established [28, 29] that when being heated, RTILs evaporate in the form of neutral ion pairs $\{[R]^+[A]^-\}_n$, where $n \geq 2$, with the subsequent dissociation of these compounds into lower-order neutral molecular complexes. Under the ion bombardment of the surfaces of ionic liquids in a high vacuum [30, 31], apart from intense peaks of cations and anions, positive and negative clusters $\{[R]^+[A]^-\}_m[R]^+$ and $\{[R]^+[A]^-\}_m[A]^-$, where $m \geq 1$, are observed in the mass spectra of sputtered (secondary) ions. Running ahead, we must note that along with cations and anions, ion beams that are obtained using ILISs contain cluster ions that are analogous to those obtained under the ion bombardment of RTILs.

At present, the 1-ethyl-3-methylglyoxaline tetrafluoroborate ionic liquid [4] is most widely used for producing ion beams. The chemical formula and molecular mass of this RTIL and the information on the cations and anions that are included in its composition are presented in Table 1, and Fig. 1 shows the cation and anion structures. Table 1 and Fig. 1 also give information on other ionic liquids that are used in ILISs. A glyoxaline-based cation enters into the composition of all aforementioned RTILs. Note that the same RTIL may be differently designated in different studies. As a rule, the full chemical name is seldom used. Instead of this, abbreviated names of cations and anions are used. For example, the aforementioned 1-ethyl-3-methylglyoxaline tetrafluoroborate ionic liquid is denoted as EMI-BF_4, or [emim][BF_4] (the cation and anion charge polarity signs are usually omitted), or [C_2mim][BF_4]. The latter name is more typical of chemical journals; here, index 2 shows the number of carbon atoms in the alkyl chain of a glyoxaline-based cation. Correspondingly, a cation [C_4mimn] with four carbon atoms in this chain is BMI or [bmin], i.e., 1-ethyl-3-methylglyoxaline. As to anions, apart from [BF_4], RTILs with [PF_6] an inorganic anion and a bis(trifluormethyl sulphonyl)imid anion are used (see

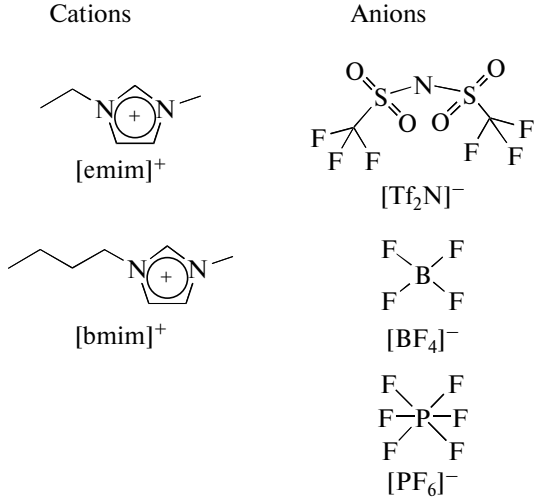

Fig. 1. Structures of cations and anions included in the composition of RTILs that are listed in Table 1.

Table 2. Physical properties of some RTILs and metals that are used in ISs [4, 32]

Substance	Density ρ, g/cm^3	Melting temperature T_m, °C	Conductivity σ, S/m	Surface tension γ, N/m	Dynamic viscosity η, Pa s
[emim][BF_4]	1.25	11	1.3	0.045	0.040
[emim][Tf_2N]	1.52	−15	0.86	0.039	0.032
[bmim][Tf_2N]	1.44	−5	0.27	0.037	0.052
[bmim][PF_6]	1.37	10	0.15	0.0475	0.350
Ga	5.91	30	>10^6	0.710	0.0019
In	7.31	157	>10^6	0.556	0.0018

Data for RTILs were obtained at room temperature; the dynamic viscosity and surface tension for metals are given at a temperature that is close to their melting temperature.

Table 1 and Fig. 1). This anion is briefly denoted as Im or [Tf_2N].

Information on some physical properties of the above RTILs is taken from [4, 32] and presented in Table 2. For comparison, the same table lists the data for gallium and indium, which are widely used in LMISs. Note that the values of the melting temperature, electrical conductivity, surface tension, and dynamic viscosity of RTILs that were obtained by different authors may differ [4].

Table 2 shows that the surface tension for RTILs is much lower than that for metals, and the dynamic viscosity is higher. As to different RTILs, an interrelation between their conductivity and dynamic viscosity is observed; namely, a decrease in the conductivity leads to an increase in the viscosity, thus being in agreement with the Walden–Pisarzhevsky rule [33] for liquid electrolytes. An increase in the molecular mass of ionic liquids is usually accompanied by a decrease in the conductivity because of a decrease in the mobility of large ions. For RTILs that are listed in Tables 1 and 2, this is valid in part.

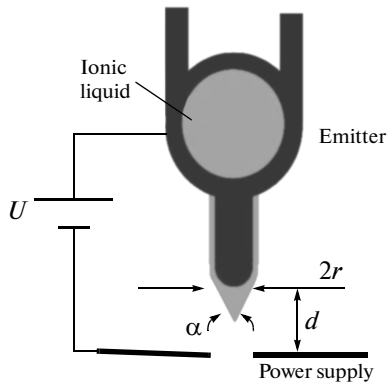

Fig. 2. Schematic image of a single needlelike IS wetted with an RTIL: (*U*) extracting voltage, (*r*) radius of the emitter tip, (*d*) distance from the emitter vertex to the grounded extractor electrode, and (α) angle of the Taylor-cone vertex.

Ionic liquids are colorless or have a slight yellowish tint, which is caused by a small content of impurities. The leading manufacturers of RTILs, e.g., the Merck firm (Germany) [34], guarantee the purity of their products at a level of 99.5% or higher. The methods for synthesizing RTILs in laboratory conditions are described in [35].

3. FEATURES OF OPERATION OF ILISS

According to Taylor's study [36], at the threshold potential difference between the electrode–extractor and the emitter tip, which is wetted with a conducting liquid, the surface of this liquid is deformed and assumes the shape of a cone (Taylor cone) with a vertex angle of $\alpha/2 = 49.3°$ (Fig. 2). The condition for the formation of such a cone is a quasi-stationary equilibrium of forces that are determined by the surface tension γ of the liquid and the action of the electric field *E*, which is directed normally to the Taylor-cone surface. If it is assumed that the emitter tip has a spherical or parabolic shape with an average radius of curvature *r*, then disregarding the effect of the space charge, the following expression can be obtained for the threshold (minimum) electric-field strength:

$$E_{\min} = \sqrt{\frac{4\gamma}{\varepsilon_0 r}}, \quad (1)$$

where ε_0 is the electric constant.

The threshold potential difference for the IS, which is schematically shown in Fig. 2, then can be calculated from the formula

$$U_{\min} = \sqrt{\frac{\gamma r}{\varepsilon_0}} \ln\frac{4d}{r}, \quad (2)$$

where *d* is the distance from the emitter tip to the extractor.

According to (2), for the radius $r = 25$ μm and distance $d = 1$ mm, the minimum potential difference $U_{\min}$ at which a Taylor cone can be formed at the emitter tip, which is wetted with the [emim][BF_4] ionic liquid, is ~1.8 kV. For liquid gallium, this potential difference is approximately 4 times larger (for the surface-

tension values taken from Table 2). It should be mentioned that the Taylor model [36] is rather simplified because it does not consider the influence of the space charge and the liquid-surface evolution in an increasing electric field; therefore, formulas (1) and (2) are based on the necessary but insufficient conditions for the formation of an equilibrium conical configuration at the emitter tip.

As in the case of liquid metals, when the electric-field strength exceeds the threshold value, field evaporation of ions from the tip of the ion-liquid-formed Taylor cone may occur, and the rate constant of this process following the Arrhenius law [37, 38] is expressed as

$$K = \nu \exp\left(-\frac{G - \sqrt{e^2 E}}{kT}\right), \quad (3)$$

where ν is the ion oscillation frequency ($\nu \sim 10^{12}$–10^{13} c^{-1} [37, 38]); k is the Boltzmann constant; T is the absolute temperature; e is the electron charge (in the case of singly charged ions); and G is the ion-evaporation activation energy. The expression under the radical sign describes a decrease in the surface barrier due to the Schottky effect [39].

The value of G for metals is calculated in the thermionic-cycle approximation [37, 38]:

$$G = \Lambda + I - W, \quad (4)$$

where Λ is the energy of the neutral-atom sublimation from the metal surface, I is the ionization energy for this atom, and W is the energy that is released when a liberated electron returns to the metal (equal to the work function for an electron leaving the metal). Note that the emitter bombardment with these electrons leads to an increase in the emitter temperature.

The main difference of the process of the field (field-ion) emission from RTILs in comparison to metals is that positively or negatively charged ions but not neutral atoms evaporate from an RTIL. By analogy to electrolyte solutions the field evaporation of ions from which was considered in detail in [40, 41], in the case of an RTIL, the value of the enthalpy change $\Delta H_{+(-)}$ upon the ion passage from the RTIL to vacuum must be substituted into formula (4) instead of the ion-evaporation activation energy.

The data on the $\Delta H_{+(-)}$ values for RTILs are absent in the available literature. Moreover, the processes of field ion evaporation from RTILs are more complex than the corresponding processes for aqueous salt solutions [40]. As during thermal evaporation of RTILs that was mentioned in Section 2, the evaporation of $\{[R]^+[A]^-\}_n$ ($n \geq 2$) neutral ion pairs with their subsequent dissociation into cations $[R]^+$ and anions $[A]^-$ is possible. Depending on the polarity of the accelerating voltage that is applied to the emitter, either cations or anions will return to the surface of the RTIL, thus initiating its etching, heating, and decomposition owing to the ion bombardment. Moreover, evaporated neutral pairs in the space near the Taylor-cone vertex can interact with the formed cations and anions; as a result, $\{[R]^+[A]^-\}_m[R]^+$ and $\{[R]^+[A]^-\}_m[A]^-$ complex ions, where $1 \leq m \leq n - 1$, will be formed.

Two main operating modes of ISs with conducting liquids must be distinguished. Depending on the values of the conductivity and surface tension of a liquid, the rate of its feeding to the emitter tip, and the electric-field strength, ISs can operate either in the pure-ion-emission mode, producing beams of singly and multiply charged atomic and cluster ions, or in the mode of emission of charged drops (a colloid source). A mixed operating mode is also possible in which a source emits both ions and charged drops.

The first mode prevails for liquid metals with conductivities $\sigma > 10^5$ S/m and high surface-tension values, and the mode of emission of charged drops with diameters of several microns is typical of electrolytes with $\sigma < 10^{-3}$ –3 S/m. This regime is also called the colloid electrospray mode [42–45].

According to their conductivities $\sigma \sim 0.1$–10 S/m and surface tensions $\gamma \sim 0.01$–0.1 N/m, ionic liquids occupy an intermediate position between liquid metals and electrolyte solutions; therefore, ILISs can operate in both modes. At a low conductivity and a high RTIL feed rate, the Taylor-cone vertex is deformed, thus leading to the formation of a thin cone jet [46, 47], flows out of the vertex (Fig. 3). The flow of emitted particles contains both charged and neutral drops and ions, as well as excited atoms and molecular complexes. Note that LMISs, including gallium ISs, for which this mode is undesirable, can also operate in the drop (colloid) mode.

The possibility of ILIS operation in the pure ion-emission mode was first experimentally confirmed in 2003 [48]. A pointed silicon-oxide capillary, through which the [emim][BF_4] RTIL was fed, served as the emitter. The inner diameter of the capillary was 30 μm, and the accelerating voltage was 1.3–2 kV. Then, Losano and Martinez-Sanchez [32] demonstrated that a source with a pointed tungsten emitter wetted with the same RTIL also can operate in the pure-ion-emission mode. The design of this IS was analogous to that schematically shown in Fig. 2. Using the same source, an ion current was obtained in [49] for different RTILs, including the [emim][BF_4] ionic liquid, which has a lower conductivity (0.34 S/m) than that for [emim][BF_4] (1.3 S/m). A [Beti] = $(C_2F_5SO_2)_2N^-$ anion with a molecular mass of 380.1 amu is similar to an [Tf_2N] anion (information on it is presented in Table 1 and Fig. 1).

In the same paper [49], the time-of-flight method was used to analyze the mass-spectral composition of the obtained ion beam. Among positive ions, apart from $[emim]^+$ ions, $\{[emim][Beti]\}_m[emim]^+$ complex ions with the maximum value of $m = 4$ (the molecular mass is 2076 amu) were recorded. In this case, the emission intensity of complex ions with $m = 1$ was higher than the cation-emission intensity. For $\{[emim][Beti]\}_m[Beti]^-$ negatively charged ions, the

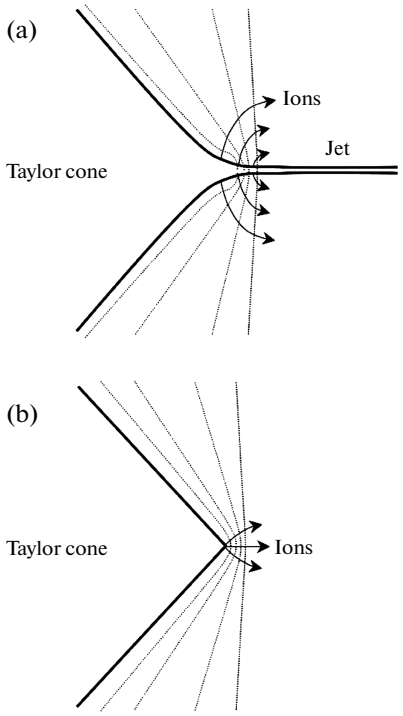

Fig. 3. Main operating modes of the ILISs: (a) drop (jet) regime and (b) purely ion-emission regime. Dotted lines show equipotential lines near the Taylor-cone vertex [46].

maximum value $m = 3$ (a molecular mass of 1854 amu) was obtained, and the anion emission intensity exceeded the emission intensity of all other ions.

It was shown in [50] that during the selection of ions of identical polarity from a needlelike source with the [emim][BF_4] RTIL, a decomposition (degradation) of this liquid occurs owing to electrochemical reactions. As a result, the withdrawn ion current decreases, and the source begins to unstably operate. The cause is that the ion liquid at the interface with a metallic electrode is depleted with ions of one polarity, thus leading to the formation of a double charged layer, which prevents the motion of ions inside the ionic liquid and initiates an accelerated destruction of the emitter tip. To eliminate this effect, it was proposed to change the polarity of the extracting voltage at the emitter at a frequency of 1 Hz. Later, a special peripheral electrode (distal electrode), to which an accelerating voltage was fed, was used to suppress electrochemical reactions [51]. An image of such a source is shown in Fig. 4. The emitter was manufactured from a porous material with dielectric properties. The concept of the distal electrode was tested not only for ILISs with single needle emitters but also for a matrix of a set of such emitters manufactured using microelectromechanical technologies.

The main part of studies that were considered above was performed and continues to be conducted at the Massachusetts Institute of Technology (MIT) (Cambridge, United States). Summarizing the achievements of this group, it can be stated that at present, isolated needlelike ISs with different RTILs can generate a stable ion current of both polarities in a range from tens of nanoamperes to units of microamperes at an accelerating voltage of several kilovolts for several hundred hours without an appreciable decomposition of the RTIL and destruction of the emitter tip. The RTIL relaxation time, i.e., the time of the source readiness for the operation after the extracting voltage is fed, is estimated at a value in a range of 0.05–0.1 ns. The electric-field strength at which the ion emission is initiated from the Taylor-cone vertex is ~1 V/nm at a radius of the emission zone of ~10 nm. The brightness of the needlelike ILIS is comparable to the brightness of a gallium liquid-metal source, and the energy spread of emitted ions is within 10 eV in the case of correctly selected operating modes.

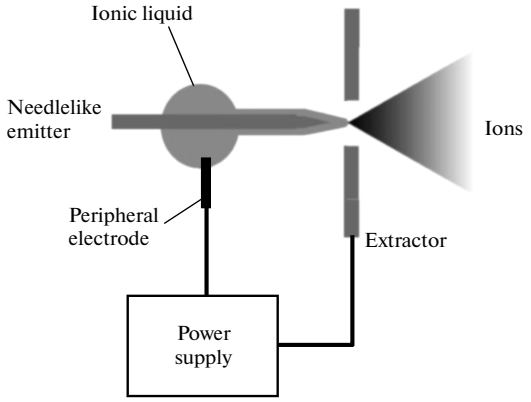

Fig. 4. An ILIS equipped with a peripheral electrode for suppressing electrochemical reactions [51].

The design of a standard ion source that operated with liquid gallium [13, 15] was taken as the basis for the design of ILISs that were used in [32, 48–51]. A special source for operation with RTILs was recently developed and tested at the Kyoto University (Japan) [52, 53]. In this source, the RTIL was fed through a steel capillary with an inner diameter of 25 μm to a porous carbon sponge with a density of 280 g/cm^3, which was closely adjacent to the pointed emitter (Fig. 5). The extractor with a 2-mm-diameter hole for ion ejection was placed at a distance of 0.5 mm from the emitter tip with a radius of curvature of ~100 μm. The experiments were performed with emitters that were produced from stainless steel, tungsten, and graphite, and the [emim][BF_4] and the [bmim][PF_6] ionic liquids, which differed in the conductivity and dynamic-viscosity values (see Table 2), served as the working substances. Preliminary measurements of the contact wetting angles showed that among the materials that were chosen for manufacturing the emitter, graphite provided the best adhesion of both RTILs with the emitter surface.

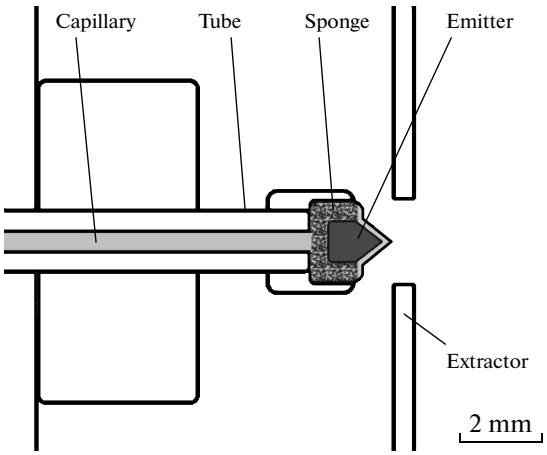

Fig. 5. An IS with a capillary for feeding an RTIL and a carbon sponge placed around the needlelike emitter [53].

The ILIS parameters were measured on the setup whose schematic diagram is shown in Fig. 6. The RTIL was injected using a syringe–pipette with a volume of 100 μL. The vacuum during measurement was no worse than 10^{-3} Pa in the chamber of the ion source and $5 \cdot 10^{-4}$ Pa in the space behind the electrostatic deflector. The total ion current was measured with a collector (Faraday cup), and the mass-spectral composition of the ion beam was determined using a time-of-flight analyzer with an ion detector on the basis of microchannel plates. Pulses of a modulating voltage with an amplitude of 1–2 kV were fed to the deflector plates; the pulse duration was 1 μs at a pulse repetition rate of 10^3 Hz.

For the [emim][BF_4] RTIL, it was found in [53] that depending on the polarity of the accelerating voltage, cations or anions predominate in the composition of ion beams with an insignificant contribution of complex molecular ions with $m = 1$ and products of the RTIL decomposition with mass numbers of 20–40 amu (Fig. 7a). On the contrary, for the [bmim][PF_6] RTIL whose conductivity is lower and dynamic viscosity is higher than for [emim][BF_4], {[bmim][PF_6]}[bmim]$^+$ and {[bmim][PF_6]}[PF_6]$^-$ ions dominate. The highest values of the ion-current density (Fig. 7b) at the best time stability of beams were obtained for graphite emitters, which, owing to their high wettability with the RTIL, provided its stable feeding to the Taylor-cone vertex. In addition, graphite is the most chemically stable substance of all that were used in this study for manufacturing emitters.

A schematic diagram of the colloid source that operates with RTILs is shown in Fig. 8 [54, 55]. This source was developed at the Institute of Advanced Industrial Science and Technology (Tsukuba, Japan). The [DEME][Tf_2N] IL, where [DEME] = $[C_8H_{20}ON]^+$, with a molecular mass of 436.43 amu and a conductivity of 0.26 S/m was used as the working substance.

The RTIL was fed through a steel capillary with an inner diameter of 30 μm, whose outlet hole was in the vacuum chamber evacuated to a pressure of 10^{-5} Pa. The capillary was at a positive (accelerating) potential relative to the extractor, which was positioned at a distance of 10 mm from the outlet hole of the capillary. The middle electrode was used to modulate the charged-particle beam; a pulsed voltage with an amplitude of up to 2.5 kV was fed to it, and the current of charged drops was measured at the collector in the regime of time-of-flight analysis.

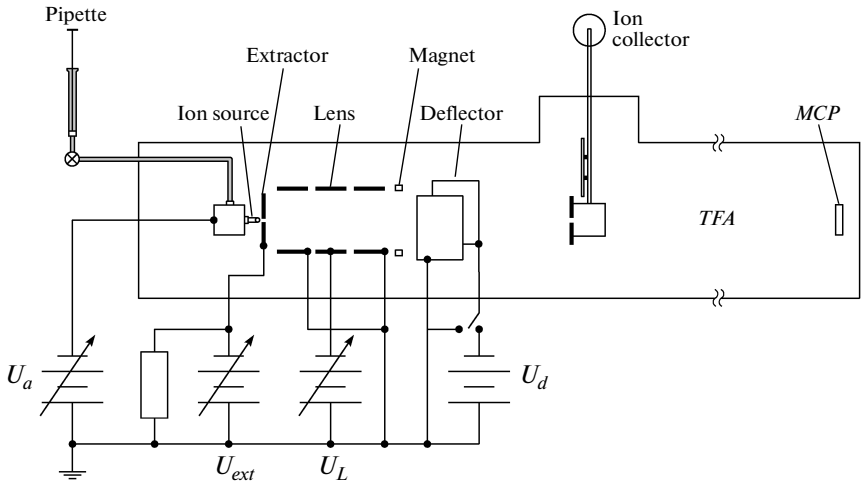

Fig. 6. Facility for investigating the ion-beam mass-spectral composition that contains an ILIS (Fig. 5), an RTIL feeding line, an ion-beam focusing and deflecting system, an ion collector (Faraday cup), a time-of-flight analyzer (TFA), and an ion detector based on microchannel plates (MCP). The distance from the end of the deflecting plates of the deflector to the ion detector (space of flight) was 1.7 m. In the negative-ion-detection mode, NdFeB-alloy magnets were used to "clear" the ion beam of electrons. The polarity of the power-supply units (U_a, U_{ext}, U_L and U_d) is presented for this regime [53].

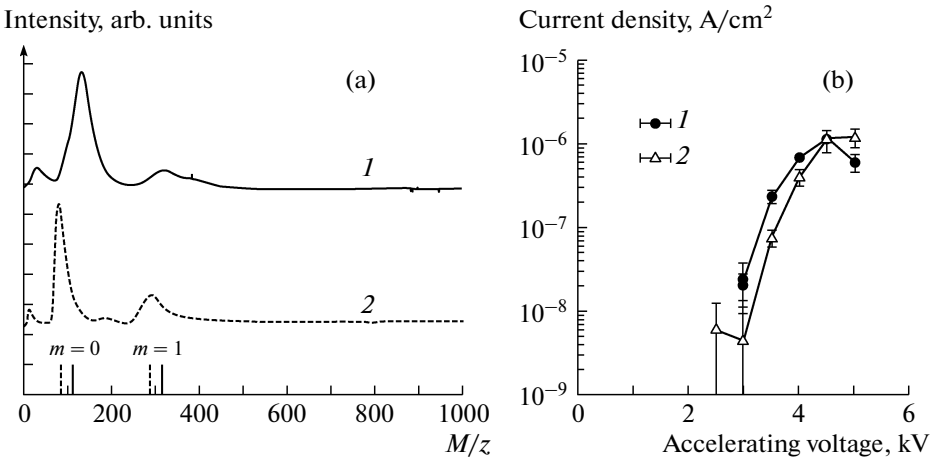

Fig. 7. Results of investigating the operation of an IS with the [emim][BF_4] RTIL and a graphite emitter (tip): (a) mass-spectral composition of a beam of positive and negative ions (M/z is the ion mass-to-charge ratio) and (b) ion-current density as a function of the accelerating voltage $|U_a - U_{ext}|$. *1* positive and (*2*) negative ions.

Figure 9 shows the experimental dependences of the drop mass-to-charge ratio M/z on the accelerating voltage and the liquid pumping rate through the capillary [55]. These measurements were performed at temperatures of 15 and 25°C. It is seen that as the accelerating voltage increases, the value of M/z decreases, while an increase in the RTIL pumping rate and a decrease in the capillary temperature have an opposite effect, and M/z increases. For $M/z = 4.3 \times 10^5$, the most probable mass of drops and their charge and diameter were estimated. It was found that the drop mass is equal to $\sim 1.8 \cdot 10^8$ amu at a charge value of 420 elementary charges and a diameter of 37 nm. If it is assumed that drops consist of neutral ion pairs with positively charged cations, the composition of drops will be $\{[\mathrm{DEME}][\mathrm{Tf_2N}]\}_{420\,000} + [\mathrm{DEME}]^+_{420}$. In this case, for an accelerating voltage of 20 keV, the average energy per mass unit (amu) of charged drops will be approximately 0.07 eV.

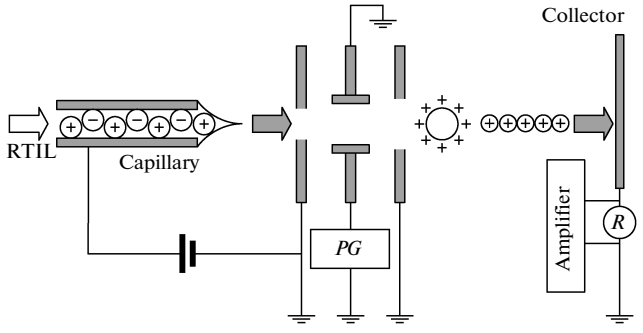

Fig. 8. High-vacuum capillary colloid source operating with RTILs: (*PG*) pulse generator and (*R*) measuring resistor in the ion-collector circuit [55].

4. MAIN FIELDS OF APPLICATION OF ION SOURCES WITH IONIC LIQUIDS

4.1. Electrostatic Rocket Engines

From the end of the 1950s to the mid-1970s, investigations on the development of electrospray (colloid) ISs for electric rocket engines were conducted. As the working substance (propellant), glycerin and other organic liquids were used. Later on, the time of LMISs came [19], which were mentioned in the introduction to this review. An interest in small electric engines has considerably increased after the advent of satellites in the CubeSat format [56, 57], which was developed in 1999 at the California Institute of Technology (Pasadena, United States) and Stanford University (Palo Alto, United States).

A CubeSat spacecraft (Fig. 10) is a metallic frame with dimensions of $10 \times 10 \times 10$ cm^3 (1U is the basic cell of CubeSat), inside which 1–2 scientific instruments with the required electronics can be placed. Solar cells that provide an energy of several watts for the satellite and telescopic antennas are placed on the outside. The total weight of the satellite does not exceed 1.33 kg. Several separate satellites can be united in a modular system (nU). Universities and commercial organizations are the main users of CubeSat satellites. Note that a more miniature format, PocketSat, has been developed by now [58].

Meanwhile, all miniature satellites are passive objects. A promising project is to equip them with electrostatic engines for correcting their orbits, precisely orienting them in the circumterrestrial space, and in the future, moving them in space, including flights to the moon and interplanetary navigation.

The first reports on the possibility of using RTLs in electrostatic rocket engines appeared in 2005 [59]. Before describing the state of the development works

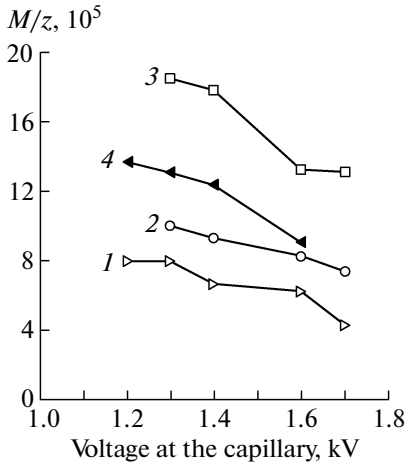

Fig. 9. Dependence of the relative mass of charged drops M/z on the accelerating voltage at the capillary for the IS (Fig. 8). The IL is [DEME][Tf_2N]. The measurement parameters: (*1*) RTIL feed rate η = 50 nL/min, the IS temperature T = 25°C; *2* – η = 100 nL/min, T = 25°C; *3* – η = 250 nL/min, T = 25°C; and *4* – η = 50 nL/min, T = 15°C.

in this field, let us refine the main characteristics of such engines [21].

The propulsive force is calculated from the formula

$$F = \frac{dm}{dt} V_{ef}, \tag{5}$$

where $\frac{dm}{dt}$ is the flow-rate propellant and V_{ef} is the average velocity of its effluence (ejection).

The specific momentum is defined as

$$I_{sp} = V_{ef}/g_0, \tag{6}$$

where g_0 is the gravitational acceleration.

Finally, the rocket-engine efficiency is

$$\eta = \frac{E_{\text{kin}}}{P_0} 100\%, \tag{7}$$

where E_{kin} is the kinetic energy of emitted particles (ions) and P_0 is the electric power of the engine, which is equal to the product of the output current by the accelerating voltage.

It was shown in [59] that a capillary source with the [emim][BF_4] ionic liquid can generate a positive-ion current of up to 4 μm at a source temperature of 120°C. Complex ions with $M/z > 600$ prevailed in the ion-beam composition, and the propulsive force was 1 μN at a specific momentum of 2000 s. Note that in rockets with engines on a chemical fuel, the specific momentum at a high propulsive force is within 450 s, and colloid sources have a specific-momentum value of ~ 1000 s. A lower value of the specific momentum I_{sp} indicates that to change the velocity of a spacecraft by the value ΔV, a larger consumption of the working substance Δm is required:

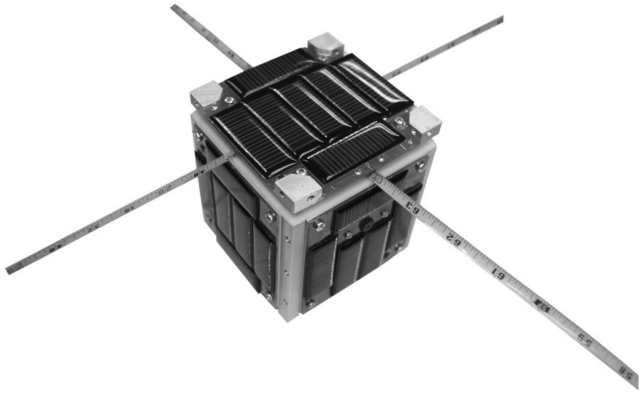

Fig. 10. A small spacecraft in the CubeSat format [57].

$$\Delta m = m_0 \left[1 - \exp\left(-\frac{\Delta V}{g_0 I_{sp}} \right) \right], \tag{8}$$

where m_0 is the initial mass of the working substance.

Formula (8) is valid for the movement of a spacecraft in open space (without an air drag). It is obvious that the specific momentum is important during long-duration expeditions, when the fuel reserve on board a spacecraft is limited. However, as follows from formulas (5)–(7), the high specific momentum restricts the propulsive force, which is necessary for putting the spacecraft into a circumterrestrial orbit. The orbit correction and changes in the satellite position require a certain propulsive force. For example, at an altitude of 600–700 km from the earth's surface, the air drag force is approximately 0.15 μN; therefore, to perform autonomous maneuvering on such an orbit, a CubeSat must have an engine with a propulsive force of several tens of micronewtons.

To provide such a propulsive force, it was proposed to create ordered structures (matrices or chips) of pointlike ILISs. A matrix source that was presented in [60] was manufactured of porous aluminum with a relative density of 55% and a diameter of pores of up to 5 μm. The source was developed at the MIT using microelectromechanical technologies. A cell of this source is shown in Fig. 11. The density of arrangement of conical emitters on the surface was 480 cm^{-2}, and the [emim][BF_4] and [emim][Tf_2N] ionic liquids were used as the working substances. It was shown that at an accelerating voltage of 1–2 kV, an isolated matrix with dimensions of 1.22 × 1.22 cm is able to generate a current of up to 400 μA. In this case, the propulsive force was 10–20 μN, and the specific momentum reached 3000 s.

A spacecraft with an electric engine that generates ions of only positive polarity will accumulate a negative charge for neutralization of which an additional source of negatively charged particles (neutralizer) is required. As a rule, a simplest electron gun is used for this purpose, which leads to a more complex engine

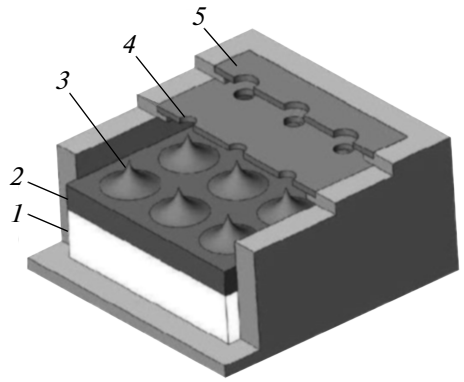

Fig. 11. A cell of the matrix IS for an electrostatic rocket engine: (*1*) reservoir with an IL, (*2*) porous matrix, (*3*) conic emitters, (*4*) extractor, and (*5*) accelerating electrode [60].

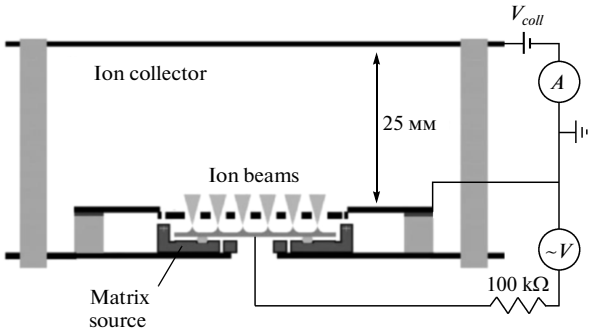

Fig. 12. Schematic of measurements of the ion current of the matrix source in the bipolar mode [60].

design and increases its mass and energy consumption. ILISs can operate in a bipolar mode, which was implemented in the proposed matrix source. The scheme of ion-current measurements in this mode is shown in Fig. 12, and the source current–voltage characteristics (CVCs) $I_{coll} = f(V_{coll})$ for operation with the [emim][BF_4] ionic liquid are shown in Fig. 13. [60]. The accelerating potential modulation frequency was 1 Hz. Despite the symmetry of the CVCs that were obtained for positive and negative ions, the full charge compensation requires a system for active emission-current control, which is currently underway at the MIT. In addition, an engine version in which an accelerating potential was applied to a peripheral electrode [51] was tested. This favored a more complete suppression of processes of electrochemical degradation of RTILs.

A similar concept of matrix electrostatic rocket engines was proposed at the Polytechnic Institute of Lausanne (Neuchatel, Switzerland) [61–63]. The engine was composed of chips, one of which is schematically shown in Fig. 14. These chips were manufactured using the newest materials and technologies. The extractor, capillaries, and chip case (Fig. 14a) were produced according to the silicon-on-insulator technology, and the chip base was manufactured of jointly baked low-temperature ceramics. The main elements of a chip are capillary emitters (Fig. 14b) that operate in the ion and microdrop generation mode (mixed mode). The inner diameter of a single capillary is 5 μm at a height of 100 μm. The density of capillary emitters in a chip (Fig. 14c) varied from 124 to 213 cm^{-2}.

It was shown [64] that a chip with 91 emitters can generate an ion current of 35 μA at an accelerating voltage of 875 V. The [emim][BF_4] and [emim][Tf_2N] ionic liquids were used as the working substances. The charge was neutralized in the bipolar regime with a low-frequency modulation of the accelerating voltage.

Preliminary estimates show that such a matrix engine with a 20-g reserve of the working substance can continuously operate for 13 000 h. In this case, the specific momentum may be as high as 3000 s, and the propulsive force amounts to 200–1500 μN (50 μN/W for an accelerating voltage of 3.8 kV). A small CubeSat satellite (3U) equipped with a similar engine cannot only successfully maneuver on circumterrestrial orbits, but can also reach the Moon's surface and participate in expeditions to Mars. The final refinement and tests of this engine were performed within the framework of the MICROTHRUST European Project [65] with participation of universities and firms from Great Britain, Netherlands, and Sweden.

Another approach to the development of an electrostatic engine with RTILs was realized at the Alta firm (Pisa, Italy) [66]. The design of the FT-150 cesium microthruster [20], which was developed at this firm within the framework of the ESA Lisa Pathfinder European Project [67], was taken as the basis. A linear (slit) IS, which was wetted with an RTIL from the inside, was used in this engine (Fig. 15). The LS plates and extractor were manufactured of stainless steel and titanium, respectively. A vessel with a volume of 50 cm^3 contained 65–67 g of the RTIL. Under the action of an electric field, many point Taylor cones (up to 100 per millimeter of the slit length) were created on the output slit of the source, thus providing its high operation efficiency.

The first tests of the linear ILIS [68] were performed with [emim][Tf_2N], and then the [emim][BF_4] RTIL was used. An accelerating voltage of ~9–12 kV was applied to the source plates, the extractor being grounded. The emission thresholds were +7 kV and –5 kV, and the ion currents for positive and negative ions were 100 and 350 μA, respectively. The IS operated in the bipolar mode at a frequency of the accelerating voltage of 0.1–1 Hz. The ion beams (depending on their polarity) contained cations, anions, and complex ions—dimers and trimmers. The IS was tested at temperatures of –30 to +70°C. It was established that an ion engine with the linear ILIS can produce a propulsive force of 100 μN at a specific

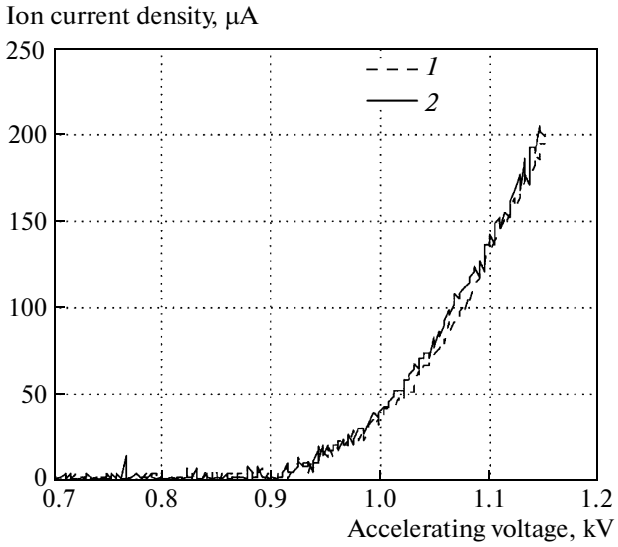

Fig. 13. The CVCs of the matrix source in the bipolar mode that were obtained during operation with the [emim][BF_4] RTIL [60]: (*1*) positive and (*2*) negative ions.

momentum of 3000 s. One of the authors of this review (A.B. Tolstogouzov) participated in the development of this IS.

4.2. Nanotechnology and Microprobe Analysis

Currently, focused gallium beams (FIBs) are used for ion lithography, precision mechanical working of materials and structures in the nanometer range, during production and retouching of photo- and X-ray masks, for reactive ion etching, and other technological operations [13, 15]. Ion sources with RTILs have a high technological potential and will be able to compete with FIBs in the nearest future.

Works on the technological application of ILISs have been performed in the recent decade [69]. It was preliminarily shown in [70] that an ILIS can provide a brightness of $(0.5–1) \times 10^6$ A cm^{-2} sr^{-1} at a width of the energy distribution of emitted ions of ~6–8 eV at a 50% level of the maximum intensity. These values are comparable to the corresponding characteristics of gallium ISs.

The gallium-emitter design (Fig. 16a) was taken as the basic construction of the technological ILIS. This source was manufactured from a 0.38-mm-diameter W wire and sharpened using the electrochemical etching method. An RTIL drop was placed in a reservoir that was manufactured from the W wire in the form of a 1.5-mm-diameter loop. The CVC of the IS during operation with the [emim][BF_4] RTIL in the mode of generation of positive ions is shown in Fig. 16b.

The ready-to-operate IS was installed in a standard FIB facility, which was developed at the CNRS/LPN (France) [72], and used for etching a silicon substrate that was covered with a mask with holes. It was shown in [71, 73] that for an accelerating potential of 15 kV, an emission current of 10 μA, and a full etching dose of $1.125 \cdot \cdot 10^{17}$ ions, the depth of the etching crater on the substrate was 17 nm. The sputtering coefficient (which is determined by the number of substance atoms that are knocked out from the target by a single ion), i.e., the etching efficiency, was found to be 5, while when operating with a 30-keV gallium beam on the same facility, the sputtering coefficient was at most 2. In this case, the rms surface roughness on the crater bottom in both cases was approximately identical, namely, 0.33 nm (ILIS) and 0.32 nm (LMIS), although an increase in the sputtering coefficient usually leads to an increase in the roughness. In the opinion of the authors of [71], the charged microdrops that were present in the beam, which was produced by an ILIS, provided smoothing of the treated surface.

A decrease in the ILIS emission current to 1 μA at the same accelerating potential and a dose of 1.125×10^{16} ions resulted in a decrease in the sputtering coefficient up to 40. Such a high etching rate cannot be obtained only due to the physical (ballistic) sputtering processes. The photoelectron-spectroscopy method was used to detect amorphization of an irradiated surface and formation of chemical compounds of silicon with carbon and nitrogen, which indicated the presence of chemical (reactive) etching of silicon. Thus, when the ILIS changes to the purely-ion-emission

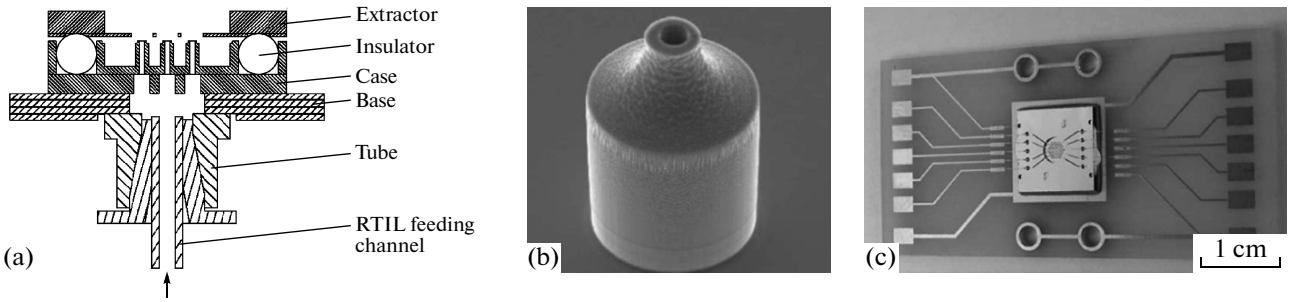

Fig. 14. Matrix electrostatic engine with capillary ISs: (a) schematic image of the chip, (b) separate capillary source, and (c) chip that is placed on a printed-circuit board [61–63].

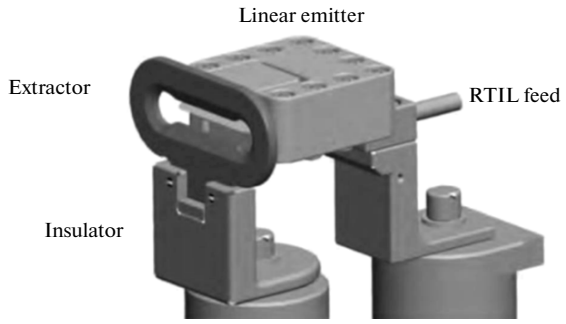

Fig. 15. A linear (slit) IS for an electrostatic rocket engine [68].

mode, bombarding ions stimulate the processes of surface disordering and formation of highly volatile silicon compounds without an additional admission of active gases of the xenon fluoride type into the chamber. Here, the further studies are aimed at equipping the FIB facility with a mass separator with crossed electric and magnetic fields (Wien filter) for reliable monitoring of the bombarding-beam composition and development of a focusing system that allows one to obtain a beam diameter of <10 nm on a sample surface. It is also presumed that an ILIS with a nanosize probing beam of positive and negative ions can be used for visualizing the surfaces of studied objects in both secondary electron-emission (scanning microscopy) and secondary ion-emission (SIMS) modes.

The capillary ILIS [52, 53] whose design is described above in Section 3 was also used in technology. It was shown in [52, 74] that under the irradiation of the surface of borosilicate glass and single-crystal silicon with ions from the source that operated with the [bmim][PF_6] RTIL, surface smoothing of the irradiated samples was observed due to the chemical sputtering, which is accompanied by the formation of free radicals (Si–F compounds), implantation of phosphorous ions, and precipitation of carbon and nitrogen, which also interacted with silicon, on the surface.

The colloid ILIS [54, 55] that was described in detail in Section 3 was intended to operate as a component of a secondary-ion mass spectrometer with an orthogonal time-of-flight analyzer. It is expected that owing to the presence of charged microdrops with $M/z > 10^5$ in the probing beam, such an IS will be especially useful in the analysis of biological objects because it will provide preservation of the molecular structure of sputtered ions. However, to date, we have no information on SIMS measurements that were performed using this IS.

5. CONCLUSIONS

The development of ISs with ILs was initiated about 10 years ago. However, despite such a short history, ILIS can even now compete with gaseous and liquid-metal ISs, especially when developing small electrostatic rocket engines. It can be expected that ILISs will be extensively introduced into modern technologies and analytical techniques, where their application only begins.

Despite a great variety of ILs, a limited number of RTILs are presently used in ISs; these are primarily [emim][BF_4] and [emim][Tf_2N]. Synthesizing new RTILs that are specially intended for generating ion beams will allow one to improve the characteristics of sources and extend their application fields.

In Russia, RTILs that were picturesquely called “liquid plasma or plasma in a bottle” still remain exotic materials, in which mainly chemists are interested. Therefore, one of the main purposes of this review was the desire to attract attention of Russian researchers to the development and application of RTILs in ion-beam and aerospace technologies, as well as in microprobe analysis. We believe that we coped with our task.

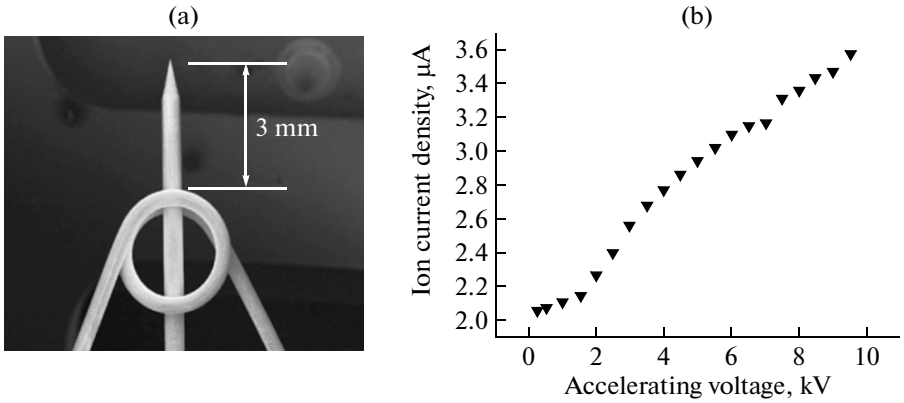

Fig. 16. An ILIS for technological applications: (a) emitter with a reservoir for RTILs; (b) CVC obtained for operation with the [emim][BF_4] RTIL in the positive-ion generation mode [71].

REFERENCES

1. Welton, T., *Chem. Rev.*, 1999, vol. 99, p. 2071, DOI: 10.102/cr980032t.
2. Wilkes, J.S., *Green Chem.,* 2002, vol. 4, p. 73, DOI: 10.1039/B110838G.
3. Rogers, R.D. and Seddon, K.R., *Science,* 2003, vol. 302, p. 792, DOI: 10.1126/science.1090313.
4. Zhang, S., Lu, X., Zhou, Q., Li, X., Zhang, X., and Li, S., *Ionic, Liquids. Physicochemical Properties* Amsterdam: Elsevier, 2009.
5. Walden, P., *Izvestiya Imperatorskoi Akademii Nauk (IV Seriya)*, 1914, vol. 8, p. 405.
6. Kustov, L.M. and Beletskaya, I.P., *Ross. Khim. Zh.*, 2004, vol. 48, p. 3.
7. Koel, M., *Crit. Rev. Anal. Chem.,* 2005, vol. 35, p. 177.
8. Bardi, U., Chenakin, S.P., Caporali, S., Lavacchi, A., Perissi, I., and Tolstogouzov, A., *Surf. Interface Anal.*, 2006, vol. 38, p. 1768, DOI: 10.1002/sia.2500.
9. *Ionic Liquids in Synthesis*, Wasserscheid, P. and Welton, T., Eds., Weinheim: Wiley-VCH, 2002.
10. Zolotov, Yu.A.*, Zh. Anal. Khim.,* 2012, vol. 67, p. 451.
11. Gabovich, M.D., *Phys.-Usp.*, 1983, vol. 26, p. 447.
12. Forbest, R.G., *Vacuum*, 1997, vol. 48, p. 85, DOI: 10.1016/Soo42-207X(96)00227-8.
13. *Introduction to Focused Ion Beams: Instrumentation, Theory, Techniques, and Practice*, Giannuzzi, L.A. and Stevie, F.A., New York: Springer-Verlag, 2005.
14. Bischoff, L., *Nucl. Instrum. Meth. Phys. Res.*, 2008, vol. 266, p. 1846, DOI: 10.1016/j.mmb.2007.12.008.
15. Orloff, J., Utlaut, M., and Swanson, L., *High Resolution Focused Ion Beams: FIB and Its Applications*, New York: Kluwer Academic, 2003.
16. Zharkov, V.V., Parshin, G.D., and Chernyak, E.Ya., *Prib. Tekh. Eksp.,* 1989, no. 1, p. 232.
17. Cherepin, V.T., Ol'khovskii, V.L., Is'yanov, V.E., Zotov, I.A., and Chenakin, S.P., *Prib. Tekh. Eksp.*, 1991, no. 4, p. 135.
18. Belykh, S.F., Evtukhov, R.N., Rasulev, U.Kh., and Redina, I.V., *Surf. Coatings Technol.*, 1992, vol. 53, p. 289, DOI: 10.1016/0257-8972(92)90388-Q
19. Rüdenauer, F.G., *Surf. Interface Anal.*, 2007, vol. 39, p. 116, DOI 10.1002/sia.2472.
20. Paita, L., Ceccanti, F., Spurio, M., Cesari, U., Priami, L., Nania, F., Rossodivita, A., and Andrenucci, M., *Proc. 31st Int. Electric Propulsion Conf. (IEPC-2009)*, Ann Arbor: Univ. Michigan, 2009.
21. Grishin, S.D. and Leskov, L.V., *Elektricheskie raketnye dvigateli kosmicheskikh apparatov* (Electrical Rocket Engines of Space Devices), Moscow: Mashinostroenie, 1989.
22. Goebel, D.M. and Katz, I., *Fundamentals of Electric Propulsions: Ion and Hall Thrusters (JPL Space Science and Technology Ser.)*, California Inst. Technol., 2008.
23. *Cluster Secondary Ion Mass Spectrometry: Principles and Applications,* Mahoney, C.M., Ed., Hoboken: Wiley, 2013.
24. Utke, I., Hoffmann, P., and Melngailis, J., *J. Vac. Sci. Technol. B: Microelectronics and Nanometer Struct.*, 2008, vol. 26, p. 1197, DOI: 10.1116/1.2955728.
25. Troyan, P.E., *Aktual'nye problemy sovremennoi elektroniki i nanoelektroniki: Uchebnoe posobie* (Actual Problems of Modern Electronics and Nanoelectronics: A Tutorial), Tomsk: TGU SUR, 2012.
26. Canongia Lopes, J.N.A. and P*á*dua, A.H., *J. Phys. Chem. B*, 2006, vol. 110, p. 3330, DOI: 10.1021/jp056006y.
27. Yang, P., Voth, G.A., Xiao, D., Hines, Jr., L.G., Bartsch, R.A., and Quitevis, E.L., *J. Chem. Phys.,* 2011, vol. 135, p. 034502, DOI: 10.1063/1.3601752.
28. Armstrong, J.P., Hurst, C., Jones, R.G., Licence, P., Lovelock, K.R.J., Satterley, C.J., and Villar-Garcia, I.J., *Phys. Chem. Chem. Phys.*, 2007, vol. 9, p. 982, DOI: 10.1039/b615137j.
29. Neto, B.A.D., Meurer, E.C., Galaverna, R., Bythell, B.J., Dupont, J., Cooks, R.G., and Eberlin, M.N., *J. Phys. Chem. Lett.*, 2012, vol. 3, p. 3435, DOI: 10.1021/jz301608c.
30. Smith, E.F., Rutten, F.J.M., Villar-Garcia, I.J., Briggs, D., and Licence, P., *Langmuir*, 2006, vol. 22, p. 9386, DOI: 10.1021/1a061248q.
31. Bundaleski, N., Caporali, S., Chenakin, S.P., Moutinho, A.M.C., Teodoro, O.M.N.D., and Tolstogouzov, A., *Int. J. Mass Spectrom.*, 2013, vol. 353, p. 19, DOI: 10.1016/j.ijms.2013.05.029
32. Losano, P. and Martínez-Sánchez, M., *J. Colloid Interface Sci.*, 2005, vol. 282, p. 415, DOI: 10.1016/j.ijis.2004.08.132.
33. Damaskin, B.B. and Petrii, O.A., *Osnovy teoreticheskoi elektrokhimii* (Foundations of Theoretical Electrochemistry), Moscow: Vyssh. Shkola, 1978.
34. http://www.merck.ru (2014).
35. Kustov, L.M., *Khimiya Zhizn'—XXI Vek*, 2007, no. 11, p. 36.
36. Taylor, G., *Proc. Royal Soc. A: Math. Phys. Eng. Sci.*, 1964, vol. 280, p. 383.
37. Müller, E.W. and Tsong, T.T., *Field Ion Microscopy*, Elsevier, 1970; Moscow: Metallurgizdat, 1972.
38. Tsong, T.T., *Atom-Probe Field Ion Microscopy*, Cambridge: Cambridge Univ., 1990.
39. Schottky, W., *Physikal. Zt.*, 1914, vol. 15, p. 872.
40. Grigor'ev, A.I., *Tech. Phys. Lett.*, 2001, vol. 27, p. 155.
41. Shiryaev, S.O., Grigor'ev, A.I., and Morozov, V.V., *Tech. Phys.*, 2003, vol. 48, p. 822.
42. Dole, M., Mack, L.L., Hines, R.L., Mobley, R.C., Ferguson, L.D., and Alice, M.B., *J. Chem. Phys.*, 1968, vol. 49, p. 2240, DOI: 10.1063/1.1670391.
43. Hagena, O.F. and Obert, W., *J. Chem. Phys.*, 1972, vol. 56, p. 1793, DOI: 10.1063/1.1677455.
44. Whitehouse, C.M., Dreyer, R.N., Yamashita, M., and Fenn, J.B., *Anal. Chem.*, 1985, vol. 57, p. 675, DOI: 10.1021/ac0028a023.
45. De la Mora, J.F. and Loscertales, I.G., *J. Fluid Mech.*, 1994, vol. 260, p. 155, DOI: 10.1017/S0022112094003472.
46. Losano, P., *J. Phys. D: Appl. Phys.*, 2006, vol. 39, p. 126, DOI 10.1088/00223727/39/1/020.
47. De la Mora, J.F., *Ann. Rev. Fluid Dynam.,* 2007, vol. 39, p. 217.

48. Romero-Sanz, I., Bocanegra, R., de la Mora, J.F., and Gamero-Castaño, M., *J. Appl. Phys.*, 2003, vol. 94, p. 3599, DOI: 10.1063/1.1598281.
49. Larriba, C., Castro, S., de la Mora, J.F., and Losano, P., *J. Appl. Phys.*, 2007, vol. 101, p. 084303, DOI: 10.1063/1.2717858.
50. Losano, P. and Martínez-Sánchez, M., *J. Colloid Interface Sci.*, 2004, vol. 280, p. 149, DOI: 10.1016/i.jcis.2004.07.037.
51. Brikner, N. and Losano, P., *Appl. Phys. Lett.*, 2012, vol. 101, p. 193504, DOI: 10.1063/1.4766293.
52. Takeuchi, M., Hamaguchi, T., Ryuto, H., and Takaoka, G.H., *Nucl. Instrum. Methods Phys. Res.*, 2013, vol. 315, p. 234, DOI: 10.1016/j.nimb.2013.04.074.
53. Takeuchi, M., Hamaguchi, T., Ryuto, H., and Takaoka, G.H., *Nucl. Instrum. Methods Phys. Res.*, 2013, vol. 315, p. 345, DOI: 10.1016/j.nimb.2013.05.065.
54. Fujiwara, Y., Saito, N., Nonaka, H., Nakanaga, T., and Ichimura, S., *Nucl. Instrum. Methods Phys. Res.,* 2010, vol. 268, p. 1938, DOI: 10.1016/j.nimb.2010.02.097.
55. Fujiwara, Y., Saito, N., Nonaka, H., and Ichimura, S., *Surf. Interf. Anal.,* 2013, vol. 45, p. 517, DOI: 10.1002/sia.5071.
56. Waydo, S., Henry, D., and Campbell, M., *IEEE Aerospace Conf. Proc.,* 2002, vol. 1, p. 435.
57. http://www.cubesat.org (2014).
58. http://www.pocketsat.org (2014).
59. Romero-Sanz, I., de Carcer, I.A., and de la Mora, J.F., *J. Propul. Power*, 2005, vol. 21, p. 239, DOI: 10.2514/1.5493.
60. Courtney, D.G., Li, H.Q., and Losano, P., *J. Phys. D: Appl. Phys.*, 2012, vol. 45, p. 485203, DOI: 10.1088/0022-3727/45/48/485203.
61. Krpoun, R. and Shea, H.R., *J. Appl .Phys.,* 2008, vol. 104, p. 064511, DOI: 10.1063/1.2981077.
62. Krpoun, R., Smith, K.L., Stark, J.P.W., and Shea, H.R., *Appl. Phys. Lett.*, 2009, vol. 94, p. 163502, DOI: 10.1063/1.3117191.
63. Krpoun, R. and Shea, H.R., *J. Micromech. Microeng.*, 2009, vol. 19, p. 045019, DOI: 10.1088/0960-1317/19/4/045019.
64. Dandavino, S., Ataman, C., Chakraborty, S., Shea, H.R., Ryan, C., and Stark, J., *Proc. 33rd Int. Electric Propulsion Conf. (IEPC-2013)*, Washington, DC: The George Washington University, 2013, p. 127.
65. http://cordis.europa.eu/projects/263035 (2014).
66. http://www.alta-space.com/ (2014).
67. http://sci.esa.int/lisa-pathfinder/ (2014).
68. Marcuccio, S., Giusti, N., and Tolstoguzov, A., *Proc. 31st Int. Electric Propulsion Conf. (IEPC-2009)*, Ann Arbor: Univ. Michigan, 2009, p. 180.
69. Perez-Martinez, C., Guilet, S., Gogneau, N., Jegou, P., Gierak, J., and Lozano, P., *J. Vac. Sci. Technol. B*, 2010, vol. 28, p. L25, DOI: 10.1116/1.3432125.
70. Zorzos, A. and Lozano, P., *J. Vac. Sci. Technol. B*, 2008, vol. 26, p. 2097, DOI: 10.1116/1.2991619.
71. Guilet, S., Perez-Martinez, C., Jegou, P., Lozano, P., and Gierak, J., *Microelectron. Eng.,* 2011, vol. 88, p. 1968, DOI: 10.1016/j.mee.2010.12.037.
72. http://www.lpn.cnrs.fr/fr/Commun/ (2014).
73. Perez-Martinez, C., Guilet, S., Gierak, J., and Lozano, P., *Microelectron. Eng.*, 2011, vol. 88, p. 2088, DOI: 101016/j.mee.2010.11.042.
74. Takaoka, G.H., Takeuchi, M., Ryuto, H., and Ueda, R., *Nucl. Instrum. Methods Phys. Res.,* 2013, vol. 315, p. 257, DOI: 10.1016/j.nimb.2012.11.072.

Translated by A. Seferov

SPELL: 1. microthrusters